Robotic vision inspection of complex joints for automatic welding

Wenyu Chen, Wei Xiong, Jierong Cheng, Ying Gu, Yusha Li
Institute for Infocomm Research, Agency for Science, Technology and Research, Singapore.
e-mail: chenw@i2r.a-star.edu.sg

***Abstract*—Automatic welding of complex joints relies on scanning and inspection of the actual joint geometry, which is important for welding path planning and welding parameter setting. A robotic vision inspection system is presented in this paper to assess the geometry of complex joints before welding. The system can scan the joint with high accuracy and high resolutions via accurate system calibration and fast data synchronization. The scanned joint geometry is inspected to assess the quality of critical dimensions. Critical features are extracted for path planning, and the joint surface is segmented into different regions for assigning different welding parameters. Experimental results based on straight-joint and Y-joint are presented to show how the proposed system works.**

Keywords-Robotic vision; geometry inspection; complex joints

I. INTRODUCTION

In shipyard shop floor, cross-tubular frame structures are common components of the jack-up legs. Welding of complex joints in such structures is usually carried out manually, as traditional welding robots cannot perform well to handle complex joint geometry conditions (Figure 1). Automatic welding robots can reduce human manual operations and improve productivity, especially in the hazardous environment. Such a kind of robots needs to automatic plan the welding trajectory, track the seams, and tune the control parameters [1]. For robotic welding of complex joints, assessments of joint geometry are required not only for trajectory planning but also for welding parameter control. Accurate welding path planning needs to be performed based on the actual joint geometry. Poorly prepared joints will be extremely difficult or even impossible for robotic welding. On the other hand, some of the welding parameters rely on the actual welding geometry [2]. For vertical and overhead regions, different parameters are required for robotic welding of the vertical and overhead seams.

(a) (b)

Figure 1 Complex joints of the jack-up legs: (a) joint before welding, and (b) joint after welding.

Some welding systems were developed using visual sensing to assist the welding. Measurement-aided welding cell (MAWC) was proposed using a multi-camera measurement system to guide the welding robots [3]. With multiple cameras surrounding the working area, the optical system provided three levels of guidance based on the measurement: pre-welding positioning, post-welding inspection, and inter-operation compensation. Such a system is not suitable for complex welding tasks such as welding of the complex joints. Visual sensors are also used for detecting the welding pool in a variable polarity plasma arc welding (VPPAW) system [4].

Instead of using 2D cameras to provide guidance, this paper presents a robotic visual inspection system using 3D sensors for actual geometry to guide the welding robot. The required geometric parameters are extracted based on the welding standard of American Welding Society (AWS) [5].

II. SYSTEM FRAMEWORK FOR COMPLEX JOINT INSPECTION

Multiple layers of welding are required to fill in the gap at the joint between two pipes (Figure 1(a)). In this paper, straight-joint and Y-joint will be used as examples, and it is assumed that 1) at least one layer has been welded manually so that the two pieces are already connected, and 2) the groove surface is the exposed surface of the top layers. Robotic visual inspection is to scan the groove geometry, then inspect and extract key points for welding path planning for the next layer. After finishing welding of the next layer, robotic visual inspection and robotic welding are performed in turns until all the layers are welded (Figure 1(b)).

Figure 2 presents the system framework for robotic visual inspection of the complex joints by scanning one layer. The system consists of two modules: data acquisition and data inspection. Data acquisition module scans the complex joint to derive a point cloud, and reconstruct a 3D surface for inspection. Data inspection module inspects the reconstructed surface, and extraction key points for both measurement and trajectory planning.

A. Data acquisition

During data acquisition, the actual welding geometry is acquired using a 3D scanning system consisting of a laser scanner and a robotic arm. To achieve high accuracy and high resolution, the system integrates the following functions:

- Calibration: performing hand-eye calibration and extract parameters for data fusion (details in Section III.A).
- Coarse-to-fine scan: performing high resolution scan in a two-step manner (details in Section III.B)
- Continuous scan: performing high speed and high resolution scan (details in Section III.C).

After scanning, the scanned data are pre-processed for shinny surface [6], followed by data fusion and surface reconstruction.

B. Data inspection

The data inspection module is able to automatically extract the groove surface from the input data, generate the perpendicular cross sections, and create key points on each cross section. These data are used for groove condition assessment and welding path planning. Six major functions are adopted to derive the desired data for groove condition assessment and welding path planning:

- Pipe fitting: the major pipe and the branch pipe are fitted to the reconstructed surface. They are used to setup the pipe coordinate system and guide the generation of the cross section following the AWS standard (details in Section IV.A).
- Groove segmentation: the reconstructed surface are segmented into four regions: one region on the major pipe, one region on the branch pipe, one region for the groove, and one region for the cutting area on the branch pipe (details in Section IV.B).
- Groove center tracking: after the groove region is identified, its center is extracted by averaging the boundary of the groove region (details in Section IV.C).
- Cross section generation: cross sections can be generated perpendicular to the groove center, or perpendicular to the intersection curve between the two pipes following the AWS standard (details in Section IV.D).
- Key point generation: four key points are obtained on each cross section (details in Section IV.E). These key points are used for groove assessment and welding path planning.
- Groove assessment: the groove angle and groove width can be derived based on the key points (details in Section IV.F).

III. DATA ACQUISITION

In this section, the setup of the data acquisition system for scanning is presented. With a track on one of the pipes, the robotic arm can rotate along the pipe and hold the scanner to scan the joint to acquire the inspection data (details in Section V.B). As an experimental setup, part of the joint will be scanned using a scanning system consists of the following components:

- Gocator 2340 profile laser sensor [7]
- ABB IRB120 robotic arm [8]
- A calibration disk with fixed diameter 100mm

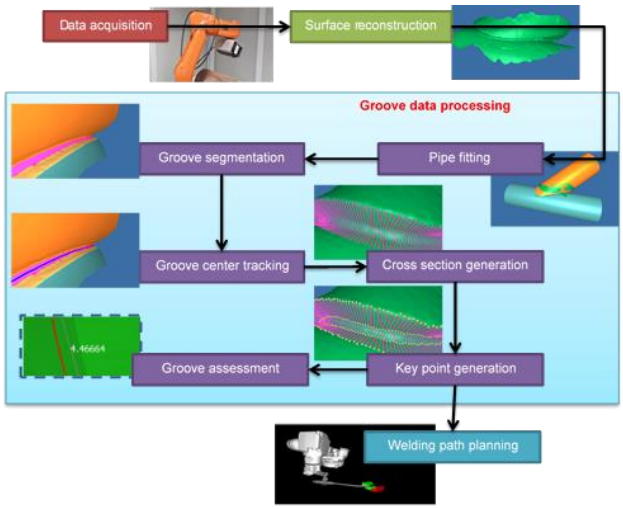

Figure 2 Robotic vision inspection of complex joints.

In the scanning system, the sensor is mounted on the TCP of the robotic arm. The robotic arm moves the sensor to different positions to scan the pipe sample. The system works in two different manners: stop-and-scan and continuous scan. In the stop-and-scan mode, the system moves the sensor to one location, stops for 0.5 second to compensate the vibration, then acquires a 3D profile. The robotic arm needs to move the sensor to different locations to acquire a set of 3D profiles, and no profile is acquired during robotic arm's movement. On the other hand, when the robotic arm moves, the continuous scan mode acquires continuous data from both the robotic arm to the sensor, and merges them together to generate a set of 3D profiles.

A. Calibration and fusion

Since the laser scanner is rigidly mounted onto the Tool Center Point (TCP) of the robotic arm, robot-sensor calibration, i.e. deriving the rigid transformation from sensor's coordinate system to TCP coordinate system, is required in order to acquire accurate three-dimensional (3D) geometry. In the experimental setup, at the *i*-th scanning position, different coordinate systems and scanned data are denoted as follow

- Φ : robotic arm's base coordinate system
- Ψ_i : TCP coordinate system
- Γ_i : sensor coordinate system
- S_i : scanned data from the sensor in Γ_i

Based on these coordinate systems, the rigid transformations are denoted as

- R_i, T_i : rotation and translation from Ψ_i to Φ ,
- R_s, T_s : rotation and translation from Γ_i to Ψ_i .

While R_i, T_i keeps changing during the scan and the value can be directly extract from the robotic arm, R_s, T_s remain fixed during data acquisition and the value can be derived as the outcome the calibration. The system adopts the disk-based calibration algorithm [9] to derive R_s, T_s .

After the calibration, putting all scanned data together in the base coordinate system gives

$$\bigcup_i \begin{pmatrix} R_i & T_i \\ 0 & 1 \end{pmatrix} \begin{pmatrix} R_s & T_s \\ 0 & 1 \end{pmatrix} \begin{pmatrix} S_i \\ 1 \end{pmatrix} = \bigcup_i \left(R_i \left(R_s S_i + T_s \right) + T_i \right). \quad (1)$$

B. *Coarse-to-fine strategy for stop-and-scan*

To reconstruct a high resolution root path, a large number of 3D profiles should be acquired. As a result, stop-and-scan mode needs a large number of locations for scanning. The coarse-to-fine strategy is designed to reduce manual work. In the coarse scan, a few locations are manually planned for the scanning system to perform a coarse scan (Figure 3(a)). The groove is segmented (Figure 3(b)) and a new path with more locations is planned (Figure 3(c,d)) for a fine scan. Then, in the fine scan, more 3D profiles are collected following the planned path (Figure 3(e)). After segmentation (Figure 3(f)), groove surface with high resolution can be acquired. The major drawback for the coarse-to-fine scanning is that it is time consuming. In the fine scan, scanning for 1200 profiles takes 10 minutes. This is mainly due to that the robotic arm needs to stop and wait before moving to the next location.

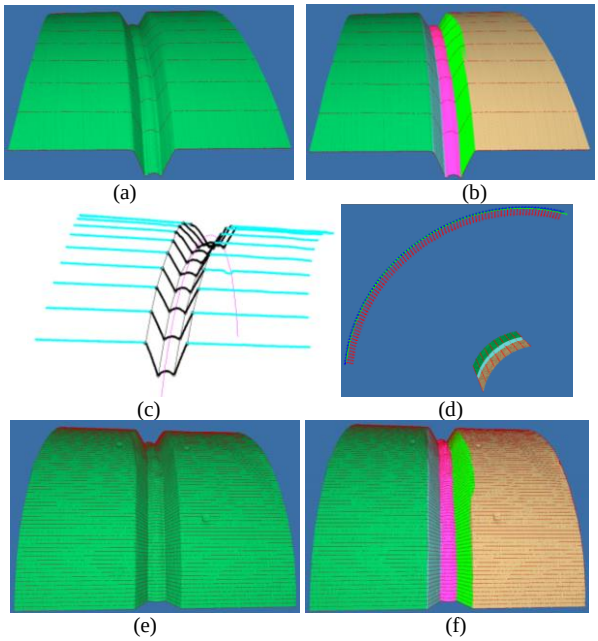

Figure 3 The coarse-to-fine scanning for a high resolution straight-joint: (a) surface from coarse scan; (b) segmentation; (c) path planning on the coarse; (d) planned path for the fine scan; (e) surface from fine scan; and (f) new segmentation.

C. *Synchronization strategy for continuous scan*

ABB Robot Reference Interface (RRI) supports data exchange on the cyclic channel, and periodically sends robot positions from the robot controller to the client. In current implementation, TCP positions are received every 4ms from RRI. On the other hand, the sensor provides one profile every 5ms. These mean that the robotic arm can provide 250 positions per second and the sensor can acquire 200 profiles per second. In general, suppose

- $\left\{\bar{R}_j, \bar{T}_j, \bar{t}_j\right\}_{j\in J}$: data received from the robotic arm, where $\bar{R}_j, \bar{T}_j$ are TCP's rotation and translation, and $\bar{t}$ is the timestamp.
- $\left[\bar{t}_{\min}, \bar{t}_{\max}\right]$: timestamp range with $\bar{t}_{\min} = \min_{j\in J}\left\{\bar{t}_j\right\}$, and $\bar{t}_{\max} = \max_{j\in J}\left\{\bar{t}_j\right\}$.
- $\left\{S_i, t_j\right\}_{i\in I}$: data received from laser sensor, where S_i is the sensor data, and t_i is its timestamp.
- $\left[t_{\min}, t_{\max}\right]$: timestamp range with $t_{\min} = \min_{i\in I}\left\{t_i\right\}$, and $t_{\max} = \max_{i\in I}\left\{t_i\right\}$.

The data from the robotic arm and the data from the sensor are of different sizes, i.e. $\|J\| \neq \|I\|$. In order to use Eq.(1) for data fusion, robot-sensor synchronization needs to generate the corresponding R_i, T_i for each S_i , which is implemented in the following steps:

Step 1: timestamps $\left\{\bar{t}_j\right\}_{j\in J}$ and $\left\{t_j\right\}_{i\in I}$ are scaled such that $\left[\bar{t}_{\min}, \bar{t}_{\max}\right] = \left[t_{\min}, t_{\max}\right] = [0,1]$.

Step 2: a 3D B-spline curve $f(\cdot)$ is generated interpolating points $\left(\bar{t}_j, \bar{T}_j\right)$ such that $f(\bar{t}_j) = \bar{T}_j$. The point T_i is taken as

$$T_i = f(t_i).$$

Step 3: represent all rotation matrices $\left\{\bar{R}_j\right\}_{j\in J}$ in quaternion form.

Step 4: for any *i*, select *j* such that $t \in \left[\bar{t}_j, \bar{t}_{j+1}\right]$. Then, the desired rotation R_i can be derived as an interpolation between $\bar{R}_j$ and $\bar{R}_{j+1}$ using the quaternion Slerp operation [10].

As presented in Figure 4(a,c), there are two different hardware setups for synchronization. In Figure 4(a), at time *T*, PC sends commands to both the robotic arm and the sensor via Ethernet. Due to unknown Ethernet delay, the timestamp for TCP position is $T+d_1$, while the timestamp for the sensor is $T+d_2$. There is a time delay between the two data: d_2-d_1. As a result, there will be bumps in the final surface as presented in Figure 4(b). In the other setup in Figure 4(c), PC sends command at time *T* to the robotic arm only, and the robotic arm triggers the sensor at time $T+d_1$ after receiving the command. Since the trigger is very faster, the timestamps of the TCP data and the profile data are almost the same, which can provide a smooth surface in Figure 4(d). The setup in Figure 4(c) is adopt in the proposed inspection system.

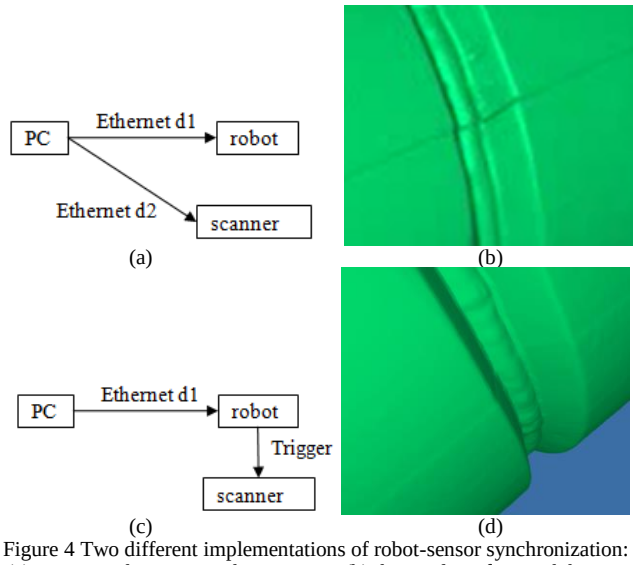

Figure 4 Two different implementations of robot-sensor synchronization: (a) system architecture without trigger, (b) the result surface with bumps (c) system architecture with trigger, and (d) the smooth surface.

D. *Comparison of two scanning manners*

Comparisons between the two different scanning strategies for scanning 1200 profiles are listed in the table below. If RRI and sensor both work at 100 Hz, continuous scan can acquire the desired 3D profiles in 12 seconds, while stop-and-scan requires 10 minutes.

TABLE I. COMPARISONS BETWEEN THE TWO STRATEGIES

	Stop-and-scan	Continuous scan
Key steps	1. Robot move to one location and stop 2. Get one profile from scanner 3. Repeat 1&2 for 1200 times	1. Start RRI and sensor 2. Robot moves TCP and triggers the sensor 3. Stop RRI and sensor 4. Merge data to get 1200 profiles
Parameters	Stops 0.5 second to reduce the vibration.	RRI: 100 Hz Sensor: 100 Hz
Timing	About 10 minutes	About 12 seconds

IV. GROOVE DATA PROCESSING

As presented in Figure 2, groove data processing is to derive the desired data for groove condition assessment, and pass data, i.e. key points for each profile, to welding path planning module. This section will introduce the six modules in the framework.

A. *Pipe fitting*

A pipe is cylinder-shaped. Thus, an algorithm to fit a cylinder to a given surface is developed. The Y-joint is reconstructed in the following steps:

- Fit a cylinder to the reconstructed surface (Figure 5(b)).
- Remove the data that belongs to the first cylinder, and fit the second cylinder to the remnant (Figure 5(c)).
- Identify one cylinder as the branch pipe, and the other one as the major pipe, such that the major pipe locates on one side of the branch pipe. As such, the Y-joint is reconstructed (Figure 5(d)).

The two cylinders will be used to guide the segmentation and build the pipe coordinate system.

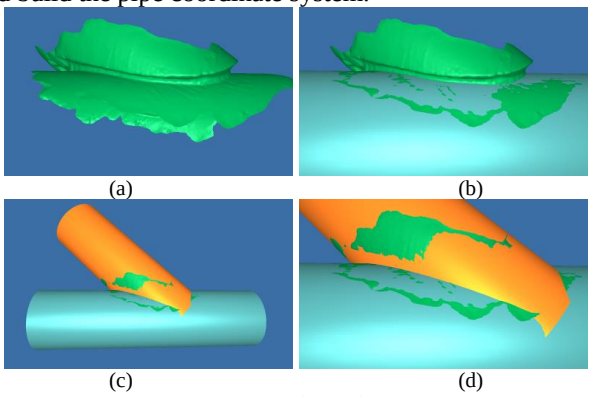

Figure 5 Major pipe and branch pipe fitting for the Y-joint: (a) reconstruct the surface; (b) fit the first cylinder; (c) fit the second cylinder; and (d) form the Y-joint.

B. *Groove segmentation*

After pipe fitting, the reconstructed surface is segmented into four parts: the major pipe surface, the branch pipe surface, the groove surface, and the cutting surface (Figure 6(b)). They can be derived as follow:

- Major pipe surface and branch pipe surface are obtained during pipe fitting.
- Remove major pipe surface and branch pipe surface from the reconstructed surface. The remnant contains both the groove surface and the cutting surface.
- Derive a feature curve along the sharp features and cut the remnant into a groove surface and a cutting surface (Figure 6(b)).

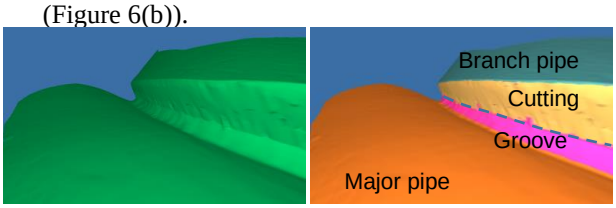

Figure 6 Y-joint surface segmentation: (a) the reconstructed surface; and (b) the segmentation.

C. *Groove centre tracking*

Generating cross sections perpendicular to the groove is equivalent to generating cross section perpendicular to the center curve of the groove surface. The groove center is tracked in three steps:

- The two boundary curves of the groove surface are extracted (Figure 7(a), the two dash curves).
- An intermediate curve is calculated from the two boundary curves. Each point P_1 on one boundary curve is projected to Q_1 on another boundary curve. The average of P_1 and Q_1 is one point on the intermediate curve. The intermediate curve is derived connecting all average points.
- The intermediate curve may not be on the groove surface. Thus, the groove center is derived as the projection of the intermediate curve onto the groove surface (Figure 7(b)).

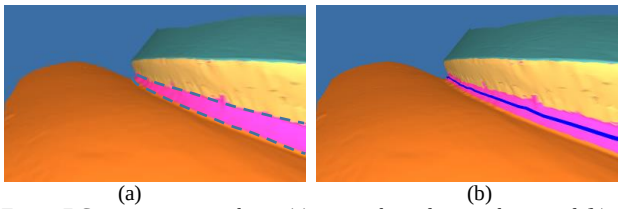

(a) (b)

Figure 7 Groove center tracking: (a) groove boundary tracking; and (b) groove center trackting.

D. *Cross sections generation*

AWS defines a way how to sample perpendicular cross section (Figure 8(a)). The proposed system samples one perpendicular cross section every one degree along the y-axis in the branch coordinate system (Figure 8(b)). The generated cross sections are finally transformed into the workpiece coordinate system (Figure 8(c)).

Figure 8(d-f) shows how the perpendicular cross sections are generated. After the sampling points on the groove center are generated, tangent directions on these points are calculated based on the groove center curve (Figure 8(d,e)). One sampling point and one tangent direction define a plane perpendicular to the groove. The intersection between the plane and the groove surface gives one perpendicular cross section (Figure 8(f)).

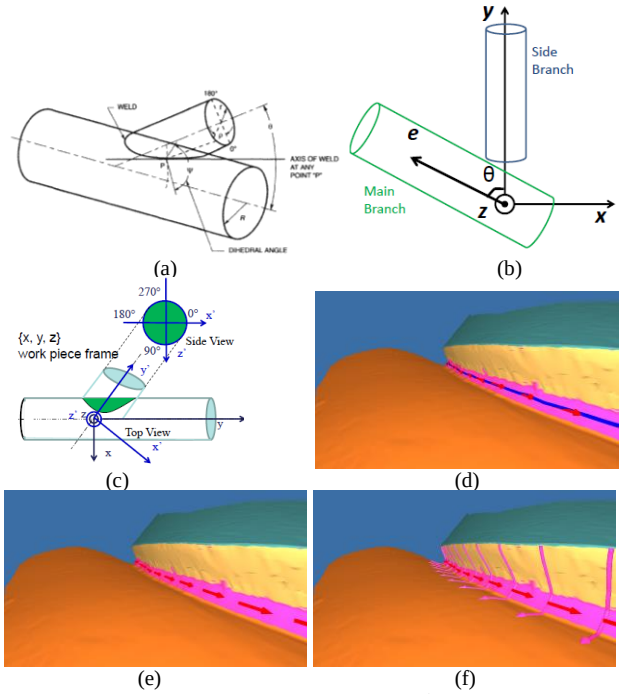

(a) (b) (c) (d) (e) (f)

Figure 8 Sampling perpendicular cross sections following AWS standard: (a) AWS definition (page 314 in [5]); (b) branch coordinate system; (c) workpiece coordinate system; (d-e) sampling points and tangent directs on the center curve; and (f) generate cross sections every one degree along the y-axis in the branch coordinate system.

E. *Key point generation*

AWS also define the way to derive the four key points. Some key points are taken as the point where the cross section passes two regions. The proposed system generates key points as follow (Figure 9).

- The starting point P_1 locates on the boundary between the branch pipe surface and the cutting surface.
- The second and the third points P_2 and P_3 are the intersections of the plane with the two boundary curve of the groove surface.
- The fourth point $P4$ locates on the major pipe surface while keeping a fixed distance to P_3.

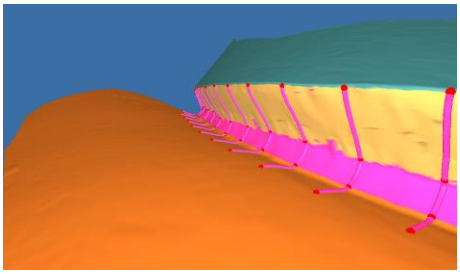

Figure 9 Four key points on each cross section

F. *Groove assessment*

Following Figure 10, groove condition are assessed based on the four key points. The opening distance is the distance between P_1 and P_4, while the groove width is the distance between P_2 and P_3. The openning angle is angle between the two lines P_2P_1 and P_3P_4.

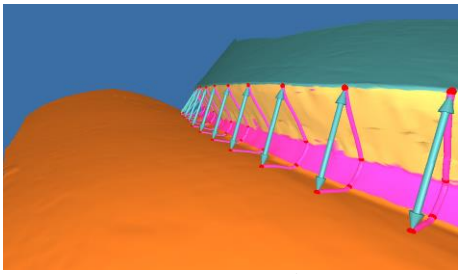

Figure 10 Groove assessment based on the four key points on each cross section: groove width and open angle

V. EXPERIMENTS

A. *Inspection of partial groove*

A demonstration system was setup to scan both a straight-joint (Figure 11(a)) and a Y-joint (Figure 11(s)). Figure 11 shows the results scanning parts of the samples. Each part is scanned following a predefined path with a few positions. With the continuous scan mode, a set of 3D profiles are acquired between two neighboring positions. All 3D profiles are combined together to form the final surface. Half of the straight-joint is scanned and reconstructed (Figure 11(b)). The reconstructed surface is automatically segmented into different patches (Figure 11(c)). For the Y-joint (Figure 11(d)), the system scanned the joint within its working range. Part of the reconstructed Y-joint is shown in Figure 11(e), which is then segmented into different areas in Figure 11(f).

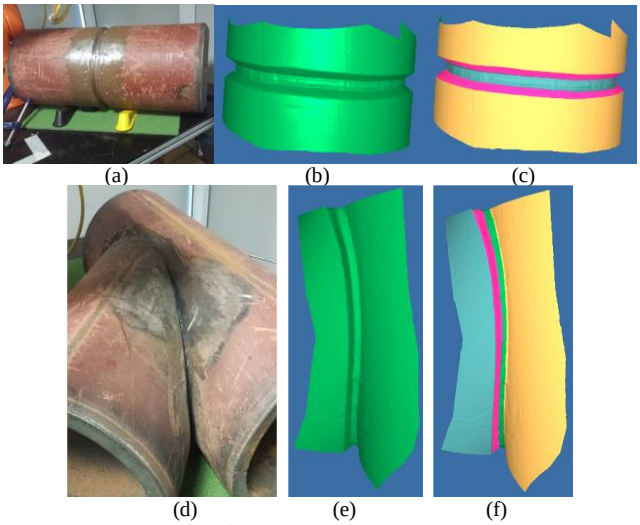

Figure 11 Current results for scanning the pipe samples. a) a straight joint (b) scan half of the joint; (c) segmentation; (d) a Y-joint; (e) scan part of Y-joint; (f) segmentation.

B. *Inspection of the whole groove*

Figure 5(a) present the reconstructed surface for a whole groove scanned using a robotic arm rotating along the branch pipe. Figure 12 shows 360 perpendicular cross sections generated after inspection, i.e. one cross section per degree. The output consists of a set of 3D data: the groove surface, the cross sections and four key points on each cross section. All data are transformed into the workpiece coordinate system.

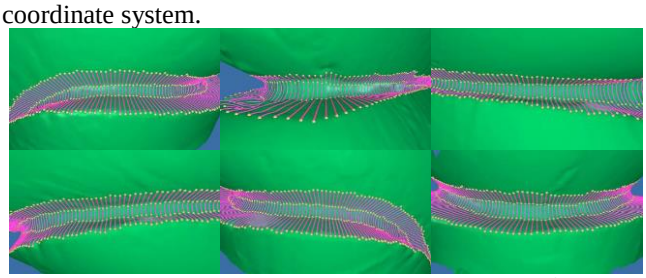

Figure 12 Groove assessment along the whole groove surface.

VI. CONCLUSIONS

A robotic vision inspection system for complex joints is presented in this paper consisting of a data acquisition module and a data processing module. Disk-based algorithm is adopt to calibrate the system, and the calibration parameters are used for data fusion. Hardware level synchronization is implemented to fuse the continuous position data from the robotic arm and continuous profile data from the scanner. Cylinder fitting is used to extract the two pipes and build the joint structure. The surface is segmented into different regions, and cross sections based on the groove surface are generated according to AWS standard. Critical features on cross sections are extracted for path planning, and segmented surface can be used for assigning different welding parameters. Experimental results based on straight-joint and Y-joint are presents.

REFERENCES

[1] T. Tarn, S. Chen, and C. Zhou, *Robotic welding, intelligence and automation* vol. 362: Springer, 2007.

[2] B. Gunnar, O. Magnus, and C. Per, "Robotic arc welding - trends and developments for higher autonomy," *Industrial Robot: the international journal of robotics research and application*, vol. 29, pp. 98-104, 2002.

[3] V. Tuominen, "The measurement-aided welding cell—giving sight to the blind," *The International Journal of Advanced Manufacturing Technology*, vol. 86, pp. 371-386, 2016.

[4] C. Jiang, F. Zhang, and Z. Wang, "Image Processing of Aluminum Alloy Weld Pool for Robotic VPPAW Based on Visual Sensing," *IEEE Access*, vol. 5, pp. 21567-21573, 2017.

[5] AWS, "D1.1-Structural Welding Code-Steel," *American Welding Society*, 2000.

[6] J. Du, W. Xiong, W. Chen, J. Cheng, Y. Wang, Y. Gu, *et al.*, "Robust laser stripe extraction using ridge segmentation and region ranking for 3D reconstruction of reflective and uneven surface," in *IEEE International Conference on Image Processing (ICIP)*, 2015, pp. 4912-4916.

[7] *LMI GOCATOR 2340*. Available: http://www.lmint.com/support/downloads/gocator-2300-family

[8] *ABB IRB 120*. Available: http://new.abb.com/products/robotics/industrial-robots/irb-120

[9] W. Chen, J. Du, W. Xiong, Y. Wang, S. Chia, B. Liu, *et al.*, "A Noise-Tolerant Algorithm for Robot-Sensor Calibration Using a Planar Disk of Arbitrary 3-D Orientation," *IEEE Transactions on Automation Science and Engineering*, vol. 15, pp. 251-263, 2018.

[10] E. B. Dam, M. Koch, and M. Lillholm, *Quaternions, interpolation and animation* vol. 2: Datalogisk Institut, Københavns Universitet Copenhagen, 1998.